Organometallics **2021**, *40*, 1765-1775

https://doi.org/10.1021/acs.organomet.1c00232

Catalytic Synthesis of Donor-Acceptor-Donor (D-A-D) and Donor-Acceptor-Acceptor (D-A-A) Pyrimidine-Ferrocenes via Acceptorless Dehydrogenative Coupling: Synthesis, Structures and Electronic Communication

Rajarshi Mondal,[a] Jason D. Braun [a] Baldeep K. Sidhu, [a] Dustin E. Nevonen, [a] Victor N. Nemykin[a,b,] and David E. Herbert [a,]**

[a] Department of Chemistry and the Manitoba Institute for Materials, University of Manitoba, 144 Dysart Road, Winnipeg, Manitoba, R3T 2N2, Canada; *david.herbert@umanitoba.ca

[b] Department of Chemistry, University of Tennessee, 1420 Circle Drive, Knoxville, Tennessee, 37996, USA; *vnemykin@utk.edu

ABSTRACT

The synthesis and full characterization of a series of ferrocene-decorated pyrimidines with donor-acceptor-donor (D-A-D) and donor-acceptor-acceptor (D-A-A) architectures is reported. The three novel compounds share a pyrimidine core and single ferrocenyl donor arm, with an additional substituent varied from donor ferrocene (**1**) to acceptor pyrenyl (**2**) to donor (4-diphenylamino)phenyl groups (**3**). The compounds could be easily constructed in acceptable yields in one-pot reactions via acceptorless dehydrogenative coupling reactions mediated by a ruthenium coordination complex supported by a simple bidentate *P^N* ligand. The solution and solid-state structures of the new pyrimidines are described along with photophysical and computational characterization. The lack of near IR (NIR) transitions upon single-electron oxidation of the compounds implies that the pyrimidinyl unit is less effective at mediating electronic communication compared with pyridine or pyrrole cores. Nevertheless, strong absorption in the far visible and NIR are observed upon formation of a dicationic species from **3** and are attributed to efficient charge-transfer from the pyrimidine core to the oxidized donor units.

INTRODUCTION

The use of π-conjugated cores to bridge electron-donating and electron-accepting groups to create symmetric (D-A-D) and asymmetric (D-A-D') donor-acceptor-donor or donor-acceptor-acceptor (D-A-A) "push-pull"-type molecules[1] is increasingly of interest in the pursuit of novel materials that can exhibit solvent-responsive fluorescence,[2] non-linear optical properties,[3–5] and the potential for mixed-valence with near infrared (NIR) absorption.[6–11] In the latter case especially, ferrocenyl moieties have been widely employed as donor units thanks to their chemical stability and stable Fe(II/III) redox couple.[12] Numerous such ferrocenyl-decorated systems have accordingly been reported, enabling studies of electronic communication across six-membered hydrocarbon[13] or heterocyclic aromatic spacers,[14] five-membered O-/N-/S-containing heterocycles,[10,11,14] triarylboranes,[15] and more extended, electron-deficient conjugated systems including boron-dipyrromethene (BODIPY),[16] aza-BODIPYs[8] and related systems,[9] and (diimine)pyridines (DIP).[17] With few exceptions,[8] these examples are generally constructed via "post-functionalization" of a previously formed π-conjugated core with a ferrocene (or other donor/acceptor appendage) using either transition metal reagents,[9] catalysts[10,11,13–15] or condensation[16,17] routes. In a similar vein, along with ferrocene-coupled arylvinyldiazene derivatives of pyrimidines,[2,18] directly coupled ferrocenyl-substituted pyrimidines have also been described (Figure 1; **A**-**G**). The synthesis of these compounds, however, again all require the use of lithioferrocene,[19] chloromercuriferrocene[20–22] or multi-step procedures via chalcone derivatives generated from acetylferrocene using Claisen-Schmidt condensation reactions.[23]

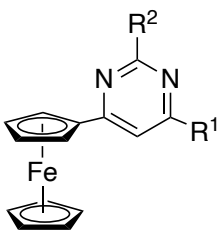

A R^1 = H, R^2 = H
B R^1 = Cl, R^2 = H
C R^1 = Cl, R^2 = Cl
D R^1 = piperidyl, R^2 = H
E R^1 = Fc, R^2 = NH_2
F R^1 = thiophen-2-yl, R^2 = NH_2
G R^1 = thiophen-2-yl, R^2 = *N*-pyrrolyl

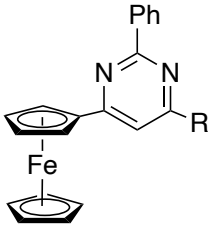

1 R = Fc
2 R = 1-pyreneyl
3 R = (4-diphenylamino)phenyl

Figure 1. Previously reported ferrocenylpyrimidines **A**,[19] **B**,[20] **C**,[21] **D**,[22] **E**[24] and **F**-**G**[23] constructed via multi-step routes and those described in this work prepared in one-pot reactions from alcohol precursors (**1**-**3**).

We recently became interested in 'acceptorless dehydrogenative coupling' (ADC) methodologies that use single-pot reactions and sustainable alcohol precursors to prepare complex *N*-heterocycles,[25] including electron-deficient heterocyclic diazines capable of mediating the sort of electronic communication described above.[26–33] These straightforward reactions are variants of the so-called "indirect" Friedländer annulation[22] that employ a single catalyst for both the oxidation of alcohols and their catalytic condensation. When employing nucleophiles such as (benz)amidines, ADC can be used to prepare a variety of highly substituted pyrimidines with only hydrogen gas and water as byproducts.[34–40] Examples include emissive variants that show pronounced solvatochromism consistent with charge-transfer character to their lowest energy excitation, derived from electronic communication across asymmetric pyrimidine-bridged donor-acceptor-donor (D-A-D') and donor-acceptor-acceptor (D-A-A) π-systems.[41] Here, we report the utility of ADC reactions for preparing ferrocene-decorated pyrimidine π-systems in one-pot. In

these complexes, ferrocenes are coupled with acceptor (pyrenyl) or donor (ferrocenyl, diarylaminophenyl) groups. In addition to their catalytic synthesis, we furthermore report their electrochemical and optical properties, computational modeling, and the solid-state structures of selected representatives. Collectively, this report is meant to highlight the utility of ADC pathways for the preparation of asymmetric ferrocene-decorated D-A-D′ and D-A-A pyrimidine π-systems.

RESULTS AND DISCUSSION

Catalytic Synthesis of Ferrocene-Pyrimidines

Compared with ADC routes to polysubstituted pyridines and quinolines, relatively fewer studies have described the synthesis of pyrimidines via homogeneous catalysis.[34–39] Recently, we disclosed a simple ruthenium hydrido chloride complex (**[Ru]**, Figure 2) bearing a bidentate diarylphosphine/phenanthridine ligand which, in conjunction with a Brønsted base, can catalyze multi-component reactions of alcohols and therefore be used to access a range of *N*-heterocycles including pyridines, quinolines and pyrimidines.[42] The ligand scaffold in **[Ru]** is notable in that it does not contain readily (de)protonated Brønsted acidic or basic groups which tend to be common in transition metal catalysts capable of these sorts of transformations, precluding a role for metal-ligand cooperativity in the catalytic ADC-type reactivity of **[Ru]**. Instead, alcohol dehydrogenation produces η^2-aldehyde adducts whose reluctance to dissociate free aldehyde is considered critical to the observed multicomponent reactivity. Targeting pyrimidines bearing ferrocenyl units, we applied previously optimized[42] one-pot catalytic conditions using both primary and secondary ferrocenyl alcohols as substrates. Benzamidine hydrochloride, α-methylferrocenemethanol and a primary alcohol (ferrocenemethanol, 1-pyrenemethanol or (4-(diphenylamino)phenyl)methanol) were combined with 0.5 mol % of **[Ru]** and KO*t*Bu and heated to reflux in dry toluene for 24 h

(Figure 2). The pyrimidine products **1**-**3** were obtained as pure orange-red solids following chromatography. The symmetric (4,6-diferrocenyl-2-phenyl)pyrimidine (**1**) was isolated in a moderate yield (45%), similar to that of the D-A-A (4-ferrocenyl-2-phenyl-6-pyrenyl)pyrimidine (**2**, 41% isolated yield). The product of the reaction of the electron-donating primary alcohol, (4-(diphenylamino)phenyl)methanol, (4-ferrocenyl-(6-*para*-(diphenylamino)phenyl)-2-phenyl)pyrimidine (**3**) was isolated in the highest yield (63%). As noted above, one-pot syntheses of ferrocene-functionalized unsymmetrical pyrimidines are relatively rare.[18]

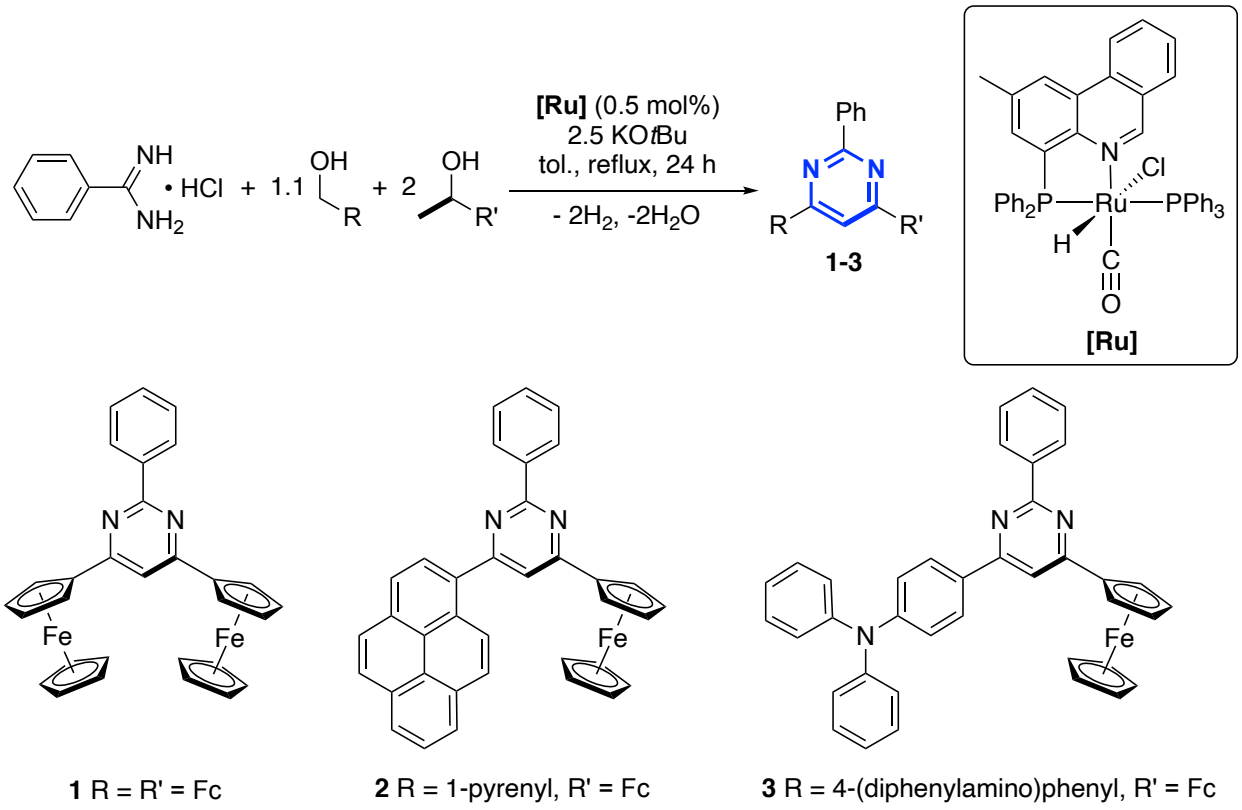

Figure 2. Synthesis of ferrocenyl-decorated pyrimidines via acceptorless dehydrogenative coupling.

Pyrimidines **1**-**3** were characterized in solution using ^{1}H and ^{13}C NMR spectroscopy, and their formulae verified by high-resolution mass spectrometry (HRMS). The ^{1}H NMR spectrum of all three products contained a distinct singlet for aromatic C*H* in the 5-position of pyrimidine core

(**1**: 7.23 ppm; **2**: 7.65 ppm; **3**: 7.20 ppm) as well as the expected signals for the cyclopentadienyl (Cp) groups of the ferrocenyl units, including a singlet for the η^5-bound ring (**1**: 4.10 ppm; **2**: 4.17 ppm; **3**: 4.11 ppm). Single crystals of **1** and **2** suitable for X-ray diffraction analysis could be grown from mixtures of dichloromethane and hexanes and confirmed the connectivity of the molecules. Figure 3a shows one of two molecules present in the asymmetric unit of **1**, while Figure 3b shows the structure of **2**. In both cases, the formation of the [N_2C_4] ring is readily apparent and its aromatic character can be deduced from the shorter C-C bond distances within the ring [**1**: C2-C3 1.386(5) and C3-C4 1.391(5) (molecule 1, shown), C32-C33 1.380(5) Å and C33-C34 1.383(5) Å (molecule 2, not shown); **2**: C2-C3 1.383(4) Å and C3-C4 1.389(4) Å] compared with the adjoining exocyclic C-C bonds [**1**: C2-C11 1.462(5) and C4-C21 1.464(5) (molecule 1, shown), C32-C41 1.471(5) Å and C34-C51 1.467(5) Å (molecule 2, not shown); **2**: C2-C11 1.483(4) Å and C4-C27 1.472(4) Å]. Both ferrocenyl units in the two molecules present in the asymmetric unit of **1** are oriented on the same side of the pyrimidinyl core, but with different degrees of twisting with respect to the C_4N_2 plane. One of the molecules (shown in Figure 3a) has a nearly flat arrangement for both ferrocenyl units (~10° with respect to the plane formed by the five carbon atoms of the adjoining Cp ring), while the second (not shown) has a more twisted conformation (~5° and 34° for the two ferrocenyl units). This suggests significant flexibility in the rotation of the connecting ferrocenyl-pyrimidinyl bonds, with the different twist angles likely dictated by packing effects. Indeed, the solid-state structure of the previously reported (6-amino-2,4-diferrocenyl)pyrimidine (**E**) has the two organometallic fragments oriented *anti* with respect to the central pyrimidinyl core.[24] In **2**, the corresponding values are ~30° for the ferrocenyl unit and ~50° for the pyrenyl unit. A similar twist of the pyrenyl unit has been reported for other pyrenyl-containing pyrimidines.[41] The phenyl

substituents in the two distinct molecules of **1** again show much smaller deviations from coplanarity with the pyrimidine core compared with **2** (~5-6° vs 30°).

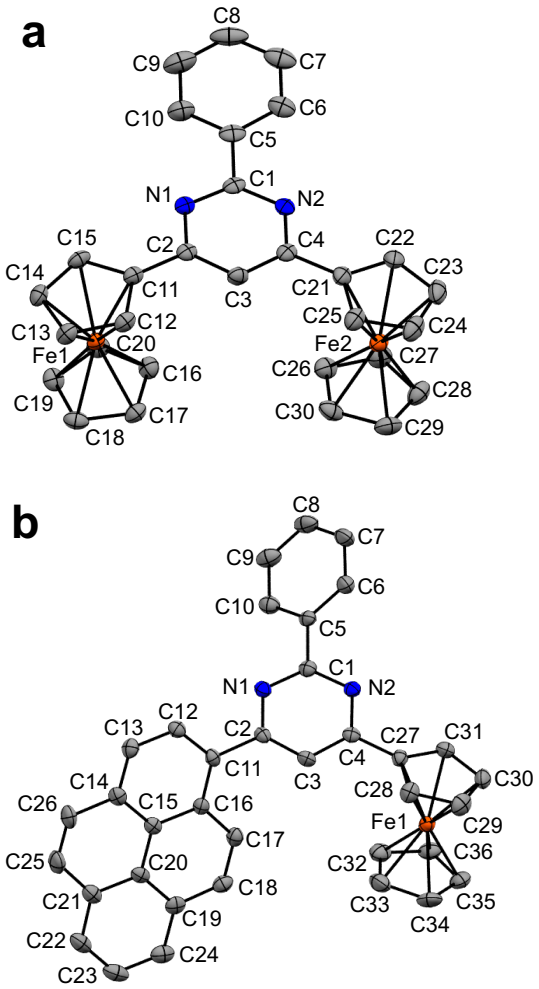

Figure 3. Solid-state structures of (a) **1** and (b) **2** with thermal ellipsoids shown at 50% probability levels. Hydrogen atoms and the second molecule in the asymmetric unit of **1** are omitted for clarity.

Photophysical and Electrochemical Properties

Absorption spectra of **1-3** in dichloromethane under ambient conditions are shown in Figure 4. The orange solids were found to be photostable in solution, with significant features in their electronic absorption spectra in both the UV and visible regions that are consistent with their color.

Notably, a prominent feature at ~350 nm (**1**: λ = 355 nm, ε = 4200 M^{-1} cm^{-1}; **2**: λ = 355 nm, ε = 22 500 M^{-1} cm^{-1}; **3**: λ = 371 nm, ε = 30 300 M^{-1} cm^{-1}) accompanies a broader and weaker lower energy absorption (**1**: 454 nm, 1600 M^{-1} cm^{-1}; **2**: 454 nm, 1100 M^{-1} cm^{-1}; **3**: 464 nm, 1800 M^{-1} cm^{-1}). Related D-A-D and D-A-A pyrimidines tend to also strongly absorb in the UV but less so in the visible region of the electromagnetic spectrum[33,41] and so the lower energy absorptions can be attributed to the presence of the organometallic fragments. In particular, the features at ~460 and ~360 nm align well with the vibronically coupled, dipole-forbidden d-d transitions of ferrocene itself (458 nm, $^1A_{1g}\rightarrow(a)^1E_{1g}$; 330 nm, $^1A_{1g}\rightarrow(b)^1E_{1g}$).[43,44] The most significant difference between the spectra is in the bathochromic shift to the 371 nm feature for **3**, which is also the most intense of the series.

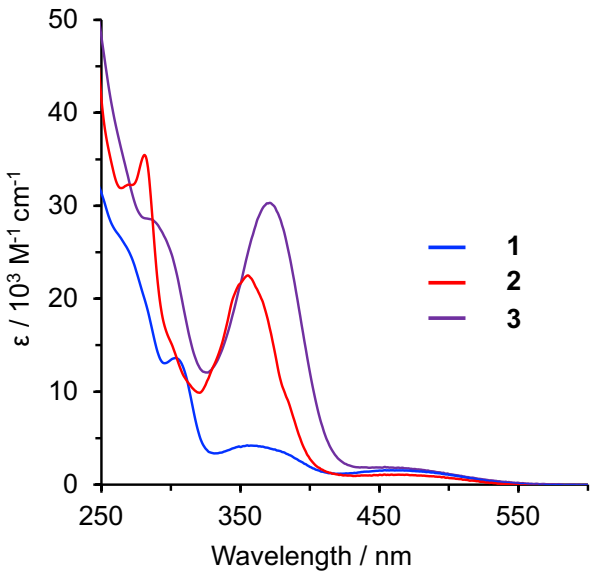

Figure 4. UV-Visible absorption spectra of 1.0 x 10^{-5} M concentration solutions of **1**-**3** in CH_2Cl_2 at 295 K.

The three pyrimidine/ferrocene compounds also show expected electrochemical behavior in solution. For **1** and **2**, a single redox event is observed at similar potentials (**1**: $E_{1/2}$ = 0.145 V; **2**: $E_{1/2}$ = 0.155 V vs $FcH^{0/+}$, FcH = ferrocene; Figure 5, Table 1), attributable to oxidation of the

ferrocenyl units. The anodic shift to these oxidation events compared to ferrocene itself is larger compared to the first ferrocenyl-based oxidation of 2,5- or 2,6-diferrocenylpyridine.[14] In fact, the redox events observed for **1** and **2** are closer to the second oxidation event observed for 2,5- or 2,6-diferrocenylpyridine (0.185 and 0.165 V vs $FcH^{0/+}$ in CH_2Cl_2 solution containing 0.1 M [*n*Bu$_4$N][B(C$_6$F$_5$)$_4$] as supporting electrolyte). This is consistent with the presence of the second nitrogen atom in the pyrimidine core compared to pyridine, which lends more electron-withdrawing character to the heteroaromatic spacer. Similarly, the first redox event observed for 2,4,6-triferrocenyl-1,3,5-triazene (0.115 V vs $FcH^{0/+}$)[14] is observed closer to those of **1** and **2**.

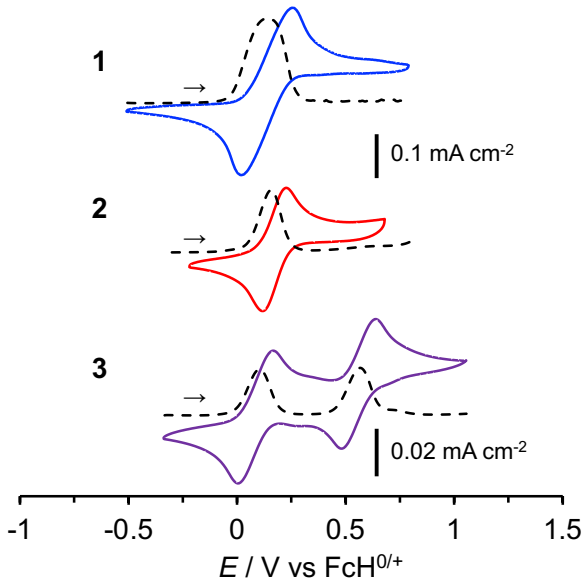

Figure 5. Cyclic voltammograms (–) and differential pulse voltammograms (---) of **1** (8.1 x 10^{-4} M), **2** (8.1 x 10^{-4} M) and **3** (1.7 x 10^{-4} M) in CH_2Cl_2 containing 0.1 M [*n*Bu$_4$N][PF_6] at 295 K: glassy carbon working electrode, a Ag/Ag^+ quasi-non-aqueous reference electrode, Pt wire counter electrode, scan rate (CV) = 100 mV s^{-1} (**1** and **2**) and 200 mV s^{-1} (**3**).

Table 1. Spectroscopic and electrochemical[a] data for **1**-**3** in CH_2Cl_2 at 295 K.

	λ / nm (ε / 10^3 $M^{-1}cm^{-1}$)	**$E_{1/2}$ / V vs $FcH^{0/+}$**
1	271 (sh), 303 (13.6), 355 (4.2), 454 (1.6)	0.145 (0.180, 0.308[b])
2	281 (35.5), 301 (sh), 355 (22.5), 454 (1.1)	0.155
3	287 (sh), 371 (30.3), 464 (1.8)	0.115, 0.585

[a] with 0.10 M [*n*Bu$_4$N][PF_6] as the supporting electrolyte using a glassy carbon working electrode and scan rates of 100 mV s^{-1}.

[b] with 0.15 M tetrabutylammonium *tetrakis*(pentafluorophenyl)borate as the supporting electrolyte using a glassy carbon working electrode and a scan rate of 25 mV s^{-1}.

Comparing the cyclic voltammograms (CVs) of **1** and **2**, the current response for **1** is twice as large as that of **2** when accounting for concentration of analyte, indicating overlapping oxidation of the two ferrocenyl units in **1** at near-identical potentials. The peak observed by differential pulse voltammetry (DPV) for **1** is also quite broad compared that of **2**. In solutions containing electrolyte comprised of weakly coordinating *tetrakis*(pentafluorophenyl)borate anions,[45] these redox events are better resolved but still quite broad ($E_{1/2}$ = 0.180, 0.308 vs $FcH^{0/+}$; Figure S1). The separation between the first and second oxidation processes of **1** (128 mV) is slightly smaller but more or less in line with those reported for 2,5- or 2,6-diferrocenylpyridine[14] and diferrocenyl BODIPY triads[46] (~150 mV). The resolution of the one-electron oxidations of the two ferrocenyl units could speak either to electronic communication[7] through the *N*-heterocyclic core or Coulombic effects dictated by electrostatic repulsion.[47,48] Related examples of cross-conjugated biferrocenes have been reported.[49,50]

Compound **3**, on the other hand, shows two well-resolved redox events. The first is consistent with oxidation of the ferrocenyl unit at similar potentials to **1** and **2** ($E_{1/2}$ = 0.115 V vs $FcH^{0/+}$). Considered as a series, the ferrocenyl oxidation correlates with the character of the other substituent: the most anodic potential is seen for **2** (bearing an electron-accepting moiety), the most cathodic potential is observed for **3** (bearing the strongest electron-donating group), while **1** is oxidized at an intermediate potential. The second redox event observed for **3** corresponds to oxidation of the diphenylamido moiety (0.585 V vs $FcH^{0/+}$). Triarylaminium cations have redox potentials spanning a wide range (~0.16-1.72 V vs $FcH^{0/+}$).[12] The observed redox potential for the $[\mathbf{3}]^{1+/2+}$ couple implies that (diphenyl)((2-ferrocenium-yl-4-phenyl)pyrimidinyl)amine can be

oxidized to form an aminyl radical at a potential intermediate between *tris*(*para*-tolyl)amine and *tris*(*para*-acylphenyl)amine.[51] A similar pair of two reversible and well-resolved oxidation processess was observed for a D-A-D' ferrocenyl-BODIPY-dimethylaminophenyl triad ($E_{1/2}$ = 0.06, 0.31 V vs $FcH^{0/+}$).[46] There, the two redox events are separated by 250 mV in CH_2Cl_2 solution (0.1 M [nBu$_4$N][ClO$_4$] as supporting electrolyte) compared with a much larger separation of 470 mV for **3**. In the former, the ferrocenyl and dimethylaminophenyl substitutents are fully conjugated into the BODIPY core via vinyl bridges. The larger physical distance between the two redox active centers confered by the bigger BODIPY core may diminish any contributions of Coloumbic repulsion to the $\Delta E_{1/2}$ compared to **3** with its smaller pyrimidine core.

To probe the spectroscopic response of **1**-**3** upon oxidation, the three compounds were subjected to oxidation under spectroelectrochemical conditions. Oxidation of **1** in this manner (Figure 6a) covering the potentials at which the redox events were observed by CV is accompanied by a decrease in intensity of the lowest energy absorption at 454 nm and the appearance in its place of a broad absorption centred at ~650 nm. This is consistent with the onset of LMCT-type transitions that lend ferrocenium its typical blue color.[44,52] Isosbestic points are evident at 431 and 518 nm. In addition, higher energy absorptions grow in intensity, with a prominent peak appearing at 265 nm and an intense shoulder at ~364 nm. The same features are observed in the presence of both hexafluorophosphate and *tetrakis*(pentafluorophenyl)borate anions (Figure S2). No significant absorption in the NIR, expected for mixed-valence biferrocenes,[53,54] was observed irrespective of the potential applied, pointing to Class I behaviour according to Robin-Day;[55] the splitting observed by electrochemistry is therefore attributable to electrostatic repulsion. A similar lack of NIR absorptions was noted in the spectroelectrochemical oxidation of the related 2,4,6-

triferrocenyl-1,3,5-triazene.[14] This contrasts the strong electronic coupling observed in NIR-absorbing tetraferrocene-decorated azadipyrromethenes.[8]

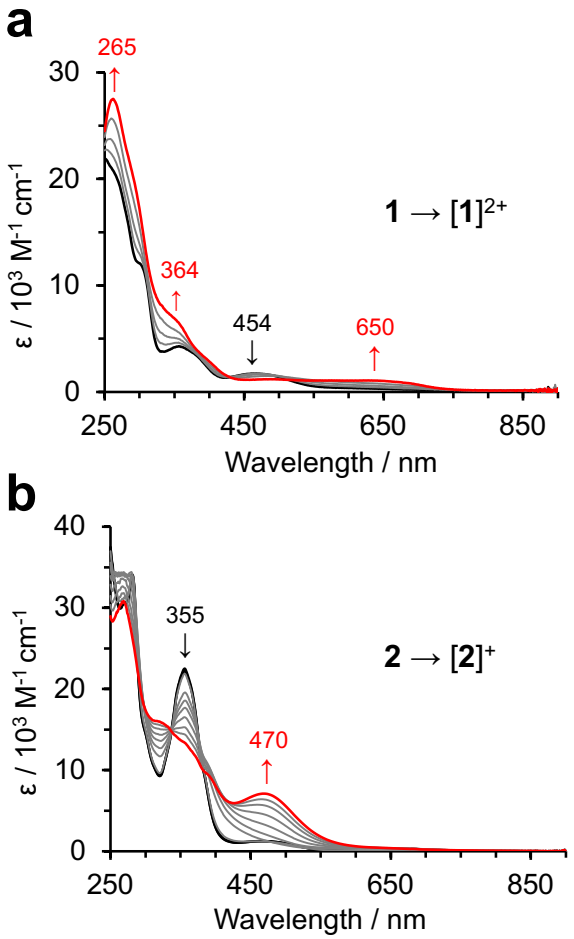

Figure 6. Spectroelectrochemical analysis of (a) **1** and (b) **2** in 0.3 M [nBu$_4$N][PF$_6$] containing CH_2Cl_2 solutions at 295 K. In both cases, the solid black trace represents the absorption spectrum at the starting potential and the red trace the absorption spectrum at the final potential, with oxidative potentials applied from (a) 0.3 V to 0.7 V and (b) 0.2 V to 1.0 V vs Ag/Ag$^+$.

In comparison, the changes in absorption upon oxidation of **2** (Figure 6b) and initial oxidation of **3** (Figure 7a) differ from those observed for **1**. Neither of these oxidatively generated electronic absorption spectra show any pronounced peaks at ~650 nm. Instead, oxidation of both compounds is accompanied by a decrease in intensity of the far UV feature (**2**: 355 nm, **3**: 371 nm) and a growth of a peak overlapping with the lowest energy absorption of the neutral species (**2**:

470 nm, **3**: shoulder at ~460 nm). Similar spectral changes were observed for oxidation of the ferrocenyl units in ferrocene-BODIPY conjugates[16,46] and related (di)ferrocenyl-substituted D-A-D triads with conjugated cores such as *bis*(difluoroboron)-1,2-*bis*{(pyrrol-2-yl)methylene}hydrazine (BOPHY).[56] In those systems, oxidation results in the appearance of a band also at shorter wavelengths compared with typical ferrocenium derivatives (~530 nm).

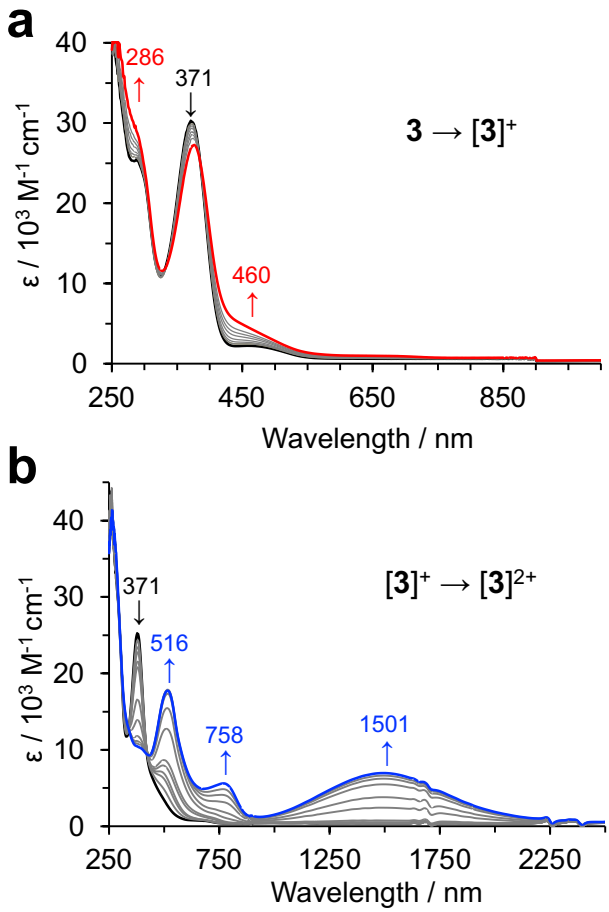

Figure 7. Spectroelectrochemical analysis of **3** in 0.3 M [*n*Bu$_4$N][PF$_6$] containing CH_2Cl_2 at 295 K. In both cases, the solid black trace represents the absorption spectrum at the starting potential and the solid colour trace the absorption spectrum at the final potential, with oxidative potentials applied from (a) 0.6 to 1.0 V and (b) 1.0 V to 1.2 V vs Ag/Ag^+.

Unique to compound **3** are the spectral changes observed upon accessing the second oxidation event seen by solution voltammetry. Figure 7b shows that upon applying increasingly

positive potentials, three new strong absorptions appear, centered at 516 nm (ε = 17 800 M^{-1} cm^{-1}), 758 nm (4 100 M^{-1} cm^{-1}), and 1501 nm (6 200 M^{-1} cm^{-1}), with a complete loss of the UV feature at 371 nm. The uniqueness of these distinctive features across the series confirms that the second redox event observed for **3** involves the diphenylaminophenyl substituent. The intensities of the new features are quite different from related compounds such as the D-A-D' ferrocenyl-BODIPY-dimethylaminophenyl triad discussed above. In that compound, low intensity NIR bands at ~1000, 1500 nm are reported to appear upon oxidation of the ferrocenyl unit but lose their intensities upon accessing the second oxidation event.[46]

DFT and TDDFT calculations

In an attempt to better understand the electronic structures, redox properties and absorption profiles of **1**-**3**, density functional theory (DFT) and time-dependent DFT (TDDFT) calculations were carried out. Optimization using the B3LYP exchange-correlation functional and PCM approach (CH_2Cl_2 as a solvent) reproduced the solid-state structural metrics of the series. Single-point and TDDFT calculations were conducted using the M06 exchange-correlation functional as it produced better agreement between theory and experiment. The D-A-D character of **1** and **3**, as well as the D-A-A character of the pyrenyl analog **2**, can be confirmed from examining the composition of the frontier molecular orbitals (MOs) of the three compounds (Figure 8 and Figure S3). Notably, the lowest unoccupied MO (LUMO) has predominantly (>50%) pyrimidine character for both **1** and **3**. As befits the D-A-A label, the pyrenyl π-system dominates the LUMO in **2** (~70%) with additional contribution from the pyrimidine core (~25%). The highest energy occupied MOs (HOMO through HOMO-4 for **1**; the HOMO through HOMO-3 for **2** and **3**) are, in each case, closely spaced. Either the highest energy (HOMO in **1** and **2**) or next highest-lying (HOMO-1 in

3) MO for all three compounds have significant ferrocene character, consistent with their solution voltammetry and spectroelectrochemical data which indicates initial oxidation of the organometallic moieties.

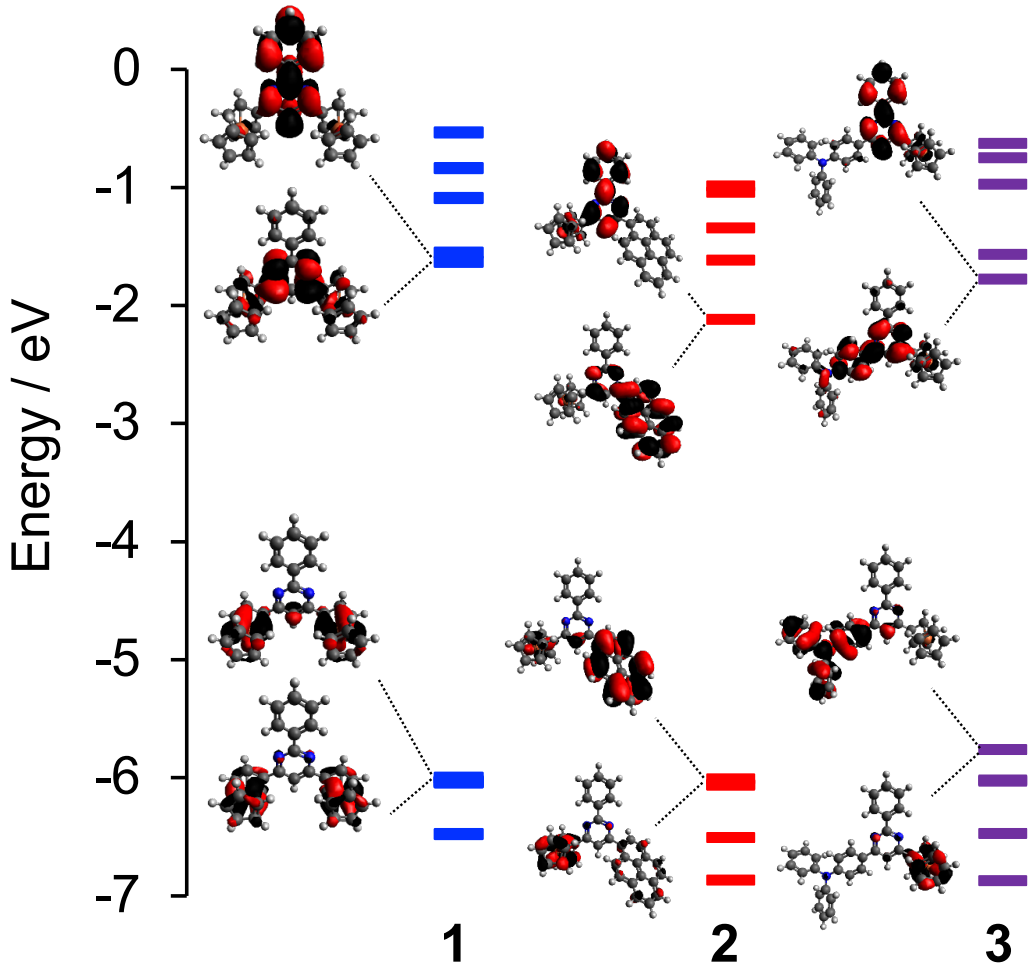

Figure 8. Molecular orbital energy level diagrams and frontier MO surfaces for **1**-**3** (M06 exchange-correlation functional) using B3LYP-optimized geometry.

It should be noted that, despite the electrochemical and spectroscopic analysis pointing towards a HOMO with ferrocene character (*vide supra*), the DFT-calculated isosurface and MO composition of the HOMO of **3** is almost exclusively (~90%) localized on the diphenylaminophenyl fragment. The energy of the HOMO in **3**, however, is very close to the

ferrocene-centered HOMO-1. A similar discrepancy was observed between the solution electrochemistry and the DFT-determined HOMO composition for a ferrocenyl-BODIPY-dimethylaminophenyl triad.[46] As noted in that work, the origin of this discontinuity could result from the choice of exchange-correlation functional. However, similar to the observations made there, all additionally exchange-correlation functionals tested here (five different functionals were tested) were still suggestive of a HOMO centered at diphenylaminophenyl fragment for B3LYP and BP86 geometries (Figures S3-S4). In addition, when spin-polarization effects were taken into consideration for [**3**]$^{+}$, DFT correctly predicted ferrocene-centered spin density in the oxidized species, supporting the applicability of our model (*vide infra*), again unsurprising as the energy difference between the (diphenylamino)phenyl-centered HOMO and ferrocene-centered HOMO-1 in **3** is very small.

Independent of the starting geometry (B3LYP or BP86), TDDFT calculations using the M06 exchange-correlation functional allowed accurate prediction of the electronic absorption spectra in **1**-**3** (assuming errors of ~0.2 eV typical of TDDFT calculations for organometallic donor-acceptor systems; Figure 9). For the calculations carried out using the M06 exchange-correlation functional and B3LYP geometries, the low-intensity lowest energy transition at ~450 nm observed for all three compounds was predicted by TDDFT as a set of several transitions with low oscillator strengths. These span between ~500-700 nm and have mixed d-d and Fc-π*(pyrimidine) character. The d-d transitions in ferrocene itself are dipole-forbidden and so are typically missed by TDDFT unless vibronic coupling is explicitly considered.[57] Indeed, predominantly d-d transitions with zero oscillator strength (transitions 1 and 2 for compound **1**, Table S1; transitions 1 and 4 for compound **2**, Table S2; and transitions 1 and 4 for compound **3**, Table S3) were predicted by TDDFT in this range. In comparison, one (excited state 5 and 2 for

compounds **1** and **2**, respectively) or two (excited states 2 and 3 for compound **3**) excited states were also calculated with oscillator strengths higher than 0.001. While these excited states also have largely ferrocene-to-ferrocene character, the d-d character is complemented by contributions from ferrocene-to-ligand single electron excitations, boosting the predicted intensity (see Supporting Information). The next lowest energy absorptions for all three compounds (~350 nm) are predicted to be largely HOMO-LUMO transitions (Tables S1-S3). These excitations have ferrocene-to-pyrimidine (**1**), ferrocene/pyrene-to-pyrene/pyrimidine (**2**) and diphenylaminophenyl/ferrocene-to-pyrimidine (**3**) charge-transfer (CT) character, respectively, explaining their stronger intensities.

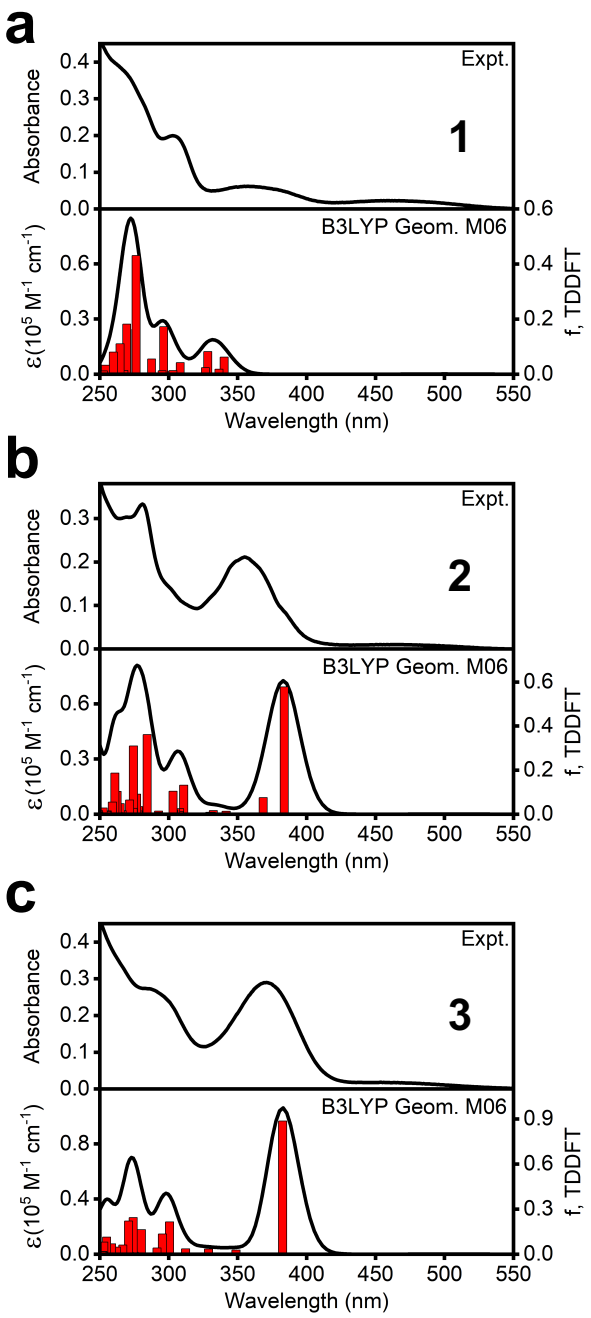

Figure 9. Experimental (upper) and TDDFT-predicted (lower) UV-vis spectra of **1**-**3** using B3LYP-optimized geometry and M06 exchange correlation functional.

To investigate the origin of the intense features observed upon spectroelectrochemical oxidation of **3**, the oxidized species $[\mathbf{3}]^{+}$ and $[\mathbf{3}]^{2+}$ were also modelled computationally as doublet

and triplet unrestricted open shells, respectively. The ground-state MO diagrams and selected orbital isosurfaces for the α and β manifolds are shown in Figure 10. Spin-density plots (Figure 11) are consistent with formation of a cation ([**3**]$^{+}$) with ferrocenium character followed by a dication ([**3**]$^{2+}$) with ferrocenium/aminyl diradical character. In terms of the electrochemically generated absorption spectra, TDDFT (Figure S7a, Table S4) attributes the growth of a shoulder at ~460 nm upon generation of [**3**]$^{+}$ to new H(β)→L+1(β)/H(α)→L+2(α) (~500 nm) and H(β)→L+1(β) (424 nm) transitions. These transitions involve transfer of electron density from the pyrimidine core and diphenylaminophenyl moieties to low-lying singly occupied molecular orbital (SOMO, here labeled as the LUMO) and fully vacant molecular orbitals (LUMO+1, LUMO+2). For the dication [**3**]$^{2+}$, these transitions are shifted to even lower energy. TDDFT suggests that the strong feature at 758 nm in Figure 7b arises from H(β)→L(β) transition involving charge-transfer between the phenylpyrimidine unit (comprising the HOMO of [**3**]$^{2+}$) and the SOMO localized on the now-oxidized diphenylaminophenyl arm (depicted in Figure 10 as L(β) of the β-manifold). The intensity of the lowest energy absorption of [**3**]$^{2+}$ at 1501 nm could not be accurately simulated, however, it is in a region characteristic of low-lying ligand-to-metal-charge transfer (LMCT) transitions reported for diferroceniumyl dications bridged by five-membered heterocycles, which can be rather intense.[11] Interestingly, in diferrocenyl-substituted oligopyrroles, extension of the heterocyclic core π-system causes a bathochromic shift in the LMCT energy while boosting its intensity. Here, the introduction of a second nitrogen in the form of a pyrimidinyl core and the substituents presumably has a similar effect of bringing the donor and acceptor orbitals in the LMCT process closer to each other in energy, resulting in an intense, low energy LMCT feature.

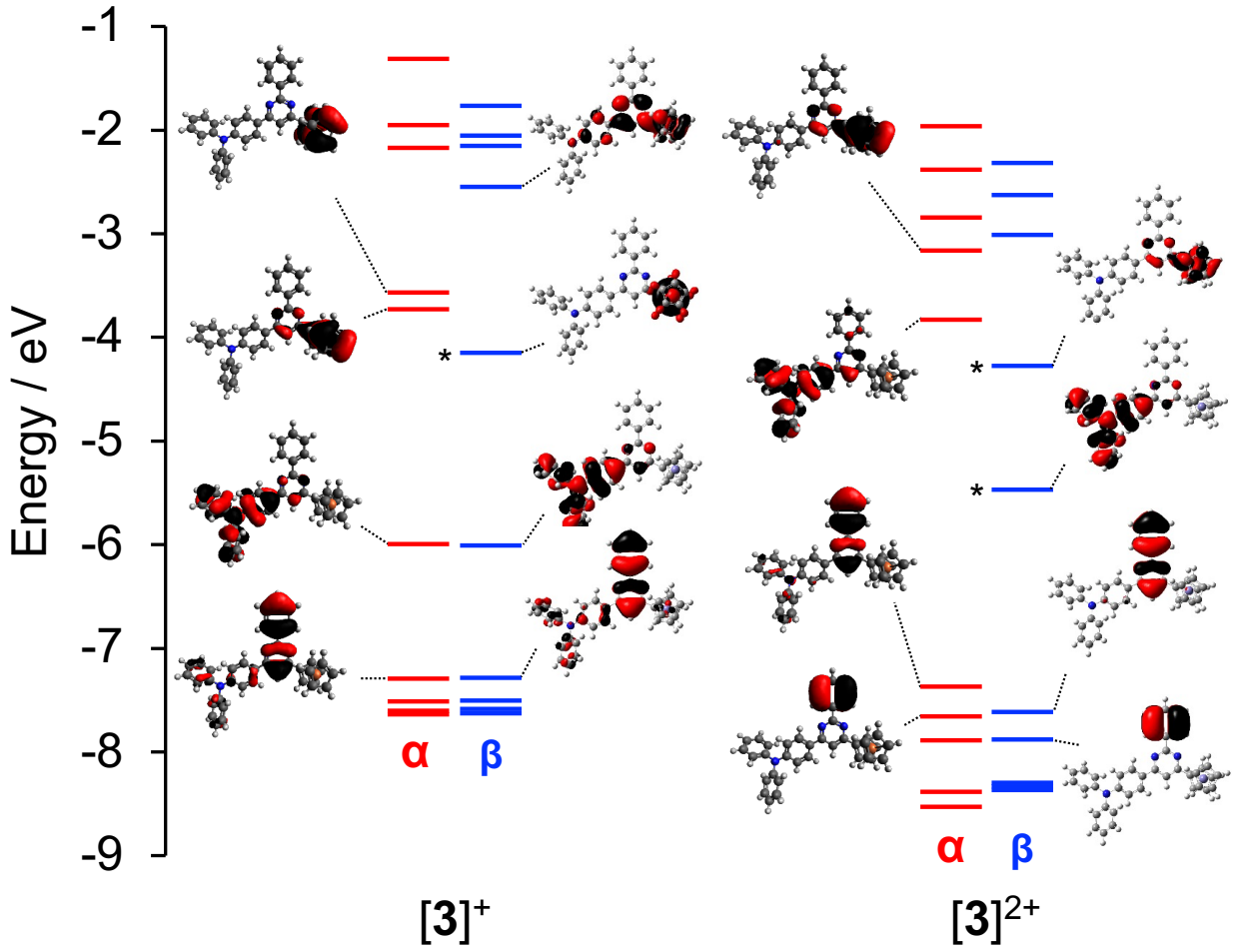

Figure 10. Energy level diagram of [**3**]$^{+}$ and [**3**]$^{2+}$ (α and β spin manifolds) and associated frontier orbitals (M06 exchange-correlation functional, unrestricted) calculated using B3LYP geometry. The orbitals associated with the electron-hole generated upon oxidation are marked with an *.

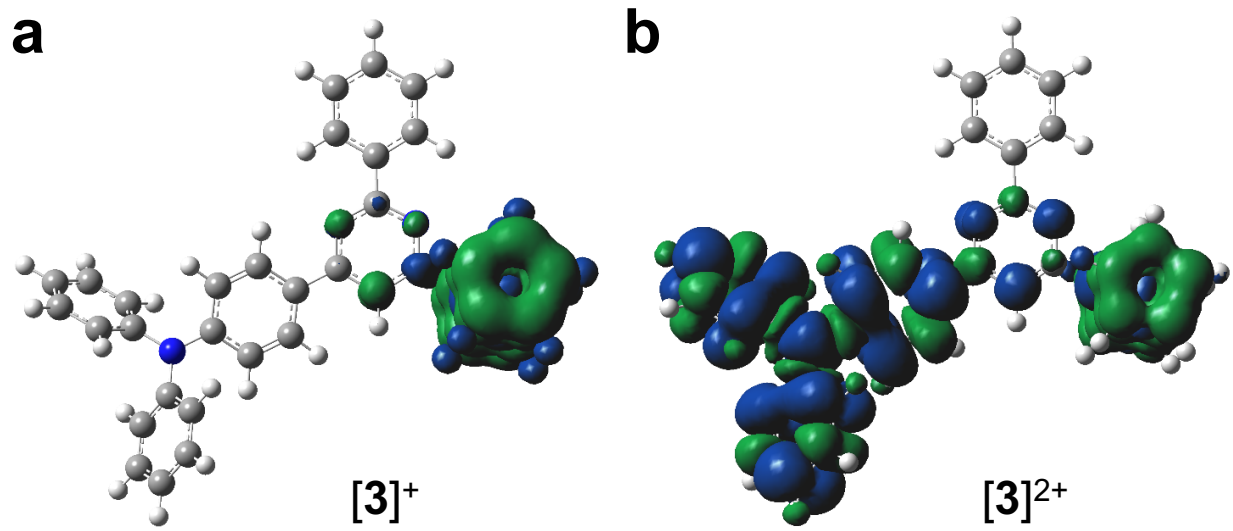

Figure 11. Total spin density plots for (a) [**3**]$^{+}$ and (b) [**3**]$^{2+}$ (M06 exchange-correlation functional) using B3LYP-optimized geometries.

Conclusions

Acceptorless dehydrogenative coupling has been shown to be a viable one-pot synthetic route to ferrocene-decorated pyrimidines starting from ferrocenyl alcohols with only dihydrogen and water produced as waste. The simultaneous construction of a conjugated pyrimidine core and appending of donor/acceptor groups enabled isolation of three examples with D-A-D (**1**), D-A-A (**2**) and D-A-D' (**3**) architectures, confirmed by single-crystal X-ray structures of **1** and **2**. All three compounds show UV-Vis absorption properties consistent with the presence of both the heterocyclic core and the organometallic side units. The redox properties of **1**-**3** were investigated using cyclic voltammetry and differential pulse voltammetry in both conventional and "weakly coordinating anion"-containing electrolytes. The first oxidation in all complexes was observed to be ferrocene-based. Compounds **1** and **3** showed a second oxidation event that, in the case of **3**, was well-resolved from the first oxidation. The overlapping oxidations of the two ferrocenyl units in **1** confirmed a lack of significant electronic communication mediated by the pyrimidine core, further supported by the absence of strong absorption features for the electrochemically generated cation $[\mathbf{1}]^{+}$. Electrochemical oxidation of **3** to $[\mathbf{3}]^{2+}$ did lead to the onset of strong features in the lower wavelength region of the visible part of the spectrum and the NIR, which were attributed to charge-transfer from the pyrimidine core to the oxidized diphenylaminyl unit rather than intervalence charge transfer. Attempts to extend ADC routes to prepare triferrocenyl analogs and analogs with alternative heterocyclic cores are presently underway.

Experimental Section

General Information

Unless otherwise stated, all air-sensitive manipulations were carried out inside an inert-atmosphere glove box (N_2) or using standard Schlenk techniques (Ar). Benzamidine hydrochloride (Combi Blocks), (1-pyrene)methanol (TCI), (ferrocene)methanol and 1-(ferrocenyl)ethanol (Millipore Sigma) were purchased as reagent grade or better and used as received. 4-(diphenylamino)phenyl)methanol[58] and the catalyst **[Ru]**[42] were prepared following published procedures. Organic solvents were dried over appropriate reagents and deoxygenated prior to use, with the exception of 1,2-dimethoxyethane, water and 2-methoxyethanol, which were simply degassed. NMR spectra were recorded on a Bruker Avance 300 MHz or Bruker Avance-III 500 MHz spectrometer as noted. Absorbance data was collected on a Cary 5000 UV-Vis NIR spectrophotometer. High-resolution mass spectra were collected on a Bruker microOTOF-QIII mass spectrometer.

For electrochemical analysis, 5-15 mg of each compound investigated was dissolved in 15 mL of 0.1 M [nBu$_4$N][PF_6] in CH_2Cl_2 and purged with Ar before analysis. All electrochemical experiments were conducted under inert (Ar) atmosphere using a CHI 760c bipotentiostat, a 3 mm diameter glassy carbon working electrode, a Ag/Ag^+ quasi-non-aqueous reference electrode separated by a Vycor tip, and a Pt wire counter electrode. Cyclic voltammetric (CV) experiments were conducted using scan rates of 50-800 mV/s. Differential pulse voltammetry (DPV) experiments were also conducted, using a 5 mV increment, 50 mV amplitude, 0.1 s pulse width, 0.0167 s sample width, and 0.5 s pulse period. Upon completion of all CV and DPV analyses, ferrocene (FcH) was added to the solution as an external standard, with all potentials reported versus the $FcH^{0/+}$ redox couple. Spectroelectrochemical measurements were conducted using a

Jasco V-770 UV-vis-NIR spectrophotometer to collect absorption data from solutions in a custom-built 1 mm cell to which a potential was applied using a CH Instruments electrochemical analyzer and a three-electrode scheme with platinum mesh working, platinum auxiliary, and a Ag/AgCl pseudo-reference electrode.

DFT and TDDFT calculations were performed using the Gaussian 16 software package.[59] The starting geometries of all compounds were optimized using the B3LYP[60,61] or BP86[62,63] exchange-correlation functional. The equilibrium geometries were confirmed with frequency calculations and more specifically, by the absence of imaginary frequencies. Iron was modeled using full-electron Wachters' basis set[64] and the other atoms were modeled using the 6-311G(d) basis set.[65] A doublet spin state was used in calculations modeling [**3**]$^{+}$, while the triplet spin state of [**3**]$^{2+}$ was found to be more energetically favorable than the open-shell singlet and thus was used for all calculations for the dication. M06 exchange correlation functional[66] was used for single-point and TDDFT calculations. For the TDDFT calculations, solvent effects were accounted for using the PCM approach[67] with CH_2Cl_2 as a solvent. The QMForge DFT analysis program[68] was used to compile molecular orbital contributions from single-point calculations.

General Synthetic Procedure: In a N_2-filled glovebox, one equivalent of benzamidine hydrochloride (0.250 mmol) was combined with KO*t*Bu (0.625 mmol) and 2 mL of dry toluene in a Schlenk flask and stirred for 20 min. Next, two equivalents of α-methylferrocenemethanol (0.500 mmol) and 1.1 equivalent of a primary alcohol (0.275 mmol) were added followed by the catalyst **[Ru]** (0.001 g, 0.001 mmol, 0.5 mol%) and an additional 2 mL of toluene. The flask was fitted with a condenser and the mixture heated in open reflux under Ar in an oil bath set to 130 °C. After

24 h, the resulting solution was cooled to ambient temperature and the product purified by silica column chromatography using a mixture of CH_2Cl_2-hexanes as the eluent.

(4,6-diferrocenyl-2-phenyl)pyrimidine (1): The general procedure was followed using benzamidine hydrochloride (0.039 g, 0.250 mmol), KO*t*Bu (0.070 g, 0.625 mmol), α-methylferrocenemethanol (0.115 g, 0.5 mmol) and ferrocenemethanol (0.059 g, 0.275 mmol). Product was eluted with a 7:3 mixture of CH_2Cl_2:hexanes (R_f = 0.47). Red solid. Yield = 0.059 g (45%). Single-crystals suitable for X-ray diffraction were grown from slow evaporation of a mixture of CH_2Cl_2 and hexanes at room temperature. ^{1}H NMR ($CDCl_3$, 300 MHz, 22 °C): δ 8.67-8.64 (m, 2H; $C_{Ph}H$), 7.58-7.48 (m, 3H; $C_{Ph}H$), 7.23 (s, 1H; $C_{pyrimidine}H$), 5.14 (m, 4H; $C_{Fc}H$), 4.52 (m, 4H; $C_{Fc}H$), 4.10 ppm (m, 10H; $C_{Fc}H$). ^{13}C{^{1}H} NMR (CD_2Cl_2, 75 MHz, 22 °C): δ 166.9 (C_{Ar}H), 163.7 (C_{Ar}), 138.8 (C_{Ar}), 130.4 (C_{Ar}H), 128.4 (C_{Ar}H), 109.6 (C_{Ar}H), 81.7 (C_{Fc}H), 70.9 (C_{Fc}H), 70.1 (C_{Fc}H), 68.2 ppm (C_{Fc}H). HRMS (ESI+) m/z calcd. For $[C_{30}H_{10}N_2Fe_2 + H]^+$ 525.0712, found 525.0766.

(4-ferrocenyl-2-phenyl-6-pyrenyl)pyrimidine (2): The general procedure was followed using benzamidine hydrochloride (0.039 g, 0.25 mmol), KO*t*Bu (0.070 g, 0.625 mmol), α-methylferrocenemethanol (0.115 g, 0.5 mmol) and 1-pyrenemethanol (0.064 g, 0.275 mmol). Product was eluted with a 1:1 mixture of CH_2Cl_2:hexanes (R_f = 0.27). Orange solid. Yield = 0.055 g (41%). Single-crystals suitable for X-ray diffraction were grown from a concentrated mixture of CH_2Cl_2 and hexanes at room temperature. ^{1}H NMR ($CDCl_3$, 300 MHz, 22 °C): δ 8.74-8.66 (overlapped m, 3H; $C_{Ph}H$, $C_{pyrene}H$), 8.34 (s, 2H; $C_{pyrene}H$), 8.28-8.24 (m, 2H; $C_{pyrene}H$), 8.19-8.16 (m, 3H; $C_{pyrene}H$), 8.09-8.04 (m, 1H; $C_{pyrene}H$), 7.65 (s, 1H; $C_{pyrimidine}H$), 7.59-7.52 (m, 3H; $C_{Ph}H$), 5.20 (m, 2H; $C_{Fc}H$), 4.57 (m, 2H; $C_{Fc}H$), 4.17 ppm (m, 5H; $C_{Fc}H$). ^{13}C{^{1}H} NMR ($CDCl_3$, 75 MHz, 22 °C): δ 168.3 (C_{Ar}), 166.2 (C_{Ar}), 164.2 (C_{Ar}), 138.4 (C_{Ar}), 134.2 (C_{Ar}), 132.3 (C_{Ar}), 131.5

(C_{Ar}), 130.9 (C_{Ar}), 130.7 (C_{Ar}H), 128.9 (C_{Ar}), 128.6 (C_{Ar}H), 128.5 (C_{Ar}H), 127.5 (C_{Ar}H), 126.4 (C_{Ar}), 125.8 (C_{Ar}), 125.5 (C_{Ar}), 125.3 (C_{Ar}), 125.0 (C_{Ar}), 124.9 (C_{Ar}), 124.8 (C_{Ar}), 115.9 (C_{Ar}), 81.3 (C_{Fc}), 71.3 (C_{Fc}H), 70.2 (C_{Fc}H), 68.4 ppm (C_{Fc}H). HRMS (ESI-TOF/MS, m/z) calcd. For $C_{30}H_{24}Fe_2N_2$ $[M]^+$, 524.0634; found 524.0616.

(4-ferrocenyl-(6-diphenylamine-2-phenyl))pyrimidine (3): The general procedure was followed using benzamidine hydrochloride (0.039 g, 0.250 mmol), KO*t*Bu (0.070 g, 0.625 mmol), α-methylferrocenemethanol (0.115 g, 0.500 mmol) and (4-(diphenylamino)phenyl)methanol (0.076 g, 0.275 mmol). Product was eluted with a 4:1 mixture of CH_2Cl_2:hexanes (R_f = 0.72). Red solid. Yield = 0.092 g (63%). ^{1}H NMR ($CDCl_3$, 300 MHz, 22 °C): 8.68 (m, 2H; $C_{Ph}H$), 8.15 (m, 2H; $C_{diphenylamine}H$), 7.53 (m, 4H; $C_{Ph}H$), 7.35-7.30 (m, 4H; $C_{diphenylamine}H$), 7.22-7.18 (overlapped m, 6H; $C_{diphenylamine}H$, $C_{pyrimidine}H$), 7.11 (m, 2H; $C_{diphenylamine}H$), 5.17 (m, 2H; $C_{Fc}H$), 4.54 (m, 2H; $C_{Fc}H$), 4.11 ppm (m, 5H; $C_{Fc}H$). ^{13}C{^{1}H} NMR ($CDCl_3$, 75 MHz, 22 °C): δ 168.2 (C_{Ar}), 163.9 (C_{Ar}), 162.8 (C_{Ar}), 150.3 (C_{Ar}), 147.3 (C_{Ar}H), 138.6 (C_{Ar}), 130.8 (C_{Ar}), 130.5 (C_{Ar}), 129.6 (C_{Ar}H), 128.5 (C_{Ar}H), 128.2 (C_{Ar}H), 125.3 (C_{Ar}H), 123.9 (C_{Ar}H), 122.4 (C_{Ar}H), 109.1(C_{Ar}), 81.7 (C_{Fc}), 71.1 (C_{Fc}H), 70.2 (C_{Fc}H), 68.3 ppm (C_{Fc}H). HRMS (ESI-TOF/MS, m/z) calcd. For $C_{38}H_{29}FeN_3$ $[M]^+$, 583.1706; found 583.1660.

X-Ray Crystallography

X-ray crystal structure data were collected from multi-faceted crystals of suitable size and quality selected from a representative sample of crystals of the same habit using an optical microscope. In each case, crystals were mounted on MiTiGen loops with data collection carried out in a cold stream of nitrogen (150 K; Bruker D8 QUEST ECO; Mo K_α radiation). All diffractometer manipulations were carried out using Bruker APEX3 software.[69] Structure solution and refinement

was carried out using XS, XT and XL,[70] embedded within OLEX2.[71] For each structure, the absence of additional symmetry was confirmed using ADDSYM incorporated in the PLATON program.[72]

Crystal structure parameters for 1 (CCDC 2069143): Red blocks; $C_{30}H_{24}Fe_2N_2$ 524.21 g/mol, orthorhombic, space group $P2_12_12_1$; a = 10.5596(5) Å, b = 12.1310(6) Å, c = 35.9691(17) Å, $\alpha = \beta = \gamma = 90°$, V = 4607.6(4) Å^3; Z = 8, ρ_{calcd} = 1.511 g cm^{-3}; crystal dimensions 0.240 x 0.080 x 0.050 mm; $2\theta_{max}$ = 55.658°; 129268 reflections, 10877 independent (R_{int} = 0.1033), intrinsic phasing; absorption coeff (μ = 1.281 mm^{-1}), absorption correction semi-empirical from equivalents (SADABS); refinement (against F_o^2) with SHELXTL V6.1, 613 parameters, 0 restraints, R_1 = 0.0390 ($I > 2\sigma$) and wR_2 = 0.0672 (all data), Goof = 1.047, residual electron density 0.35/−0.38 Å^{-3}.

Crystal structure parameters for 2 (CCDC 2069144): Orange blocks; $C_{36}H_{24}FeN_2$ 540.42 g/mol, orthorhombic, space group *Pbca*; a = 13.2254(6) Å, b = 10.8909(5) Å, c = 34.5653(14) Å, $\alpha = \beta = \gamma = 90°$, V = 4978.7(4) Å^3; Z = 8, ρ_{calcd} = 1.442 g cm^{-3}; crystal dimensions 0.400 x 0.150 x 0.070 mm; $2\theta_{max}$ = 50.242°; 85534 reflections, 4429 independent (R_{int} = 0.1180), intrinsic phasing; absorption coeff (μ = 1.281 mm^{-1}), absorption correction semi-empirical from equivalents (SADABS); refinement (against F_o^2) with SHELXTL V6.1, 352 parameters, 0 restraints, R_1 = 0.0529 ($I > 2\sigma$) and wR_2 = 0.0976 (all data), Goof = 1.101, residual electron density 0.29/−0.33 Å^{-3}.

ASSOCIATED CONTENT

Supporting Information. Multi-nuclear NMR and HRMS spectra of all new compounds; additional computational plots and figures and computational coordinates; and crystallographic

information files containing all X-ray data. CCDC 2069143-2069144 contain the supplementary crystallographic data for this paper. The data can be obtained free of charge from The Cambridge Crystallographic Data Center via www.ccdc.cam.ac.uk/structures.

The following files are available free of charge:

Supporting Information File (PDF)

Crystallographic Information Files (CIF)

AUTHOR INFORMATION

Corresponding Author

David E. Herbert (david.herbert@umanitoba.ca)

Victor N. Nemykin (vnemykin@utk.edu)

ORCIDs

Rajarshi Mondal: 0000-0002-6819-6690

Jason D. Braun: 0000-0002-5850-8048

Baldeep K. Sidhu: 0000-0002-2016-6601

Dustin E. Nevonen: 0000-0002-6049-5418

Victor Nemykin: 0000-0003-4345-0848

David E. Herbert: 0000-0001-8190-2468

Author Contributions

The manuscript was written through contributions of all authors. All authors have given approval to the final version of the manuscript.

Conflicts of Interest

There are no conflicts of interest to declare.

ACKNOWLEDGMENTS

We gratefully acknowledge the Natural Sciences Engineering Research Council of Canada for a Discovery Grant to DEH (RGPIN-2014-03733); the Canadian Foundation for Innovation and Research Manitoba for an award in support of an X-ray diffractometer (CFI #32146); the University of Manitoba for GETS/SEGS support (RM, JDB, BKS); and Compute Canada for access to computational resources.

REFERENCES

(1) Bureš, F. Fundamental Aspects of Property Tuning in Push–Pull Molecules. *RSC Adv.* **2014**, *4*, 58826–58851.

(2) Vidal, M.; Pastenes, C.; Rezende, M. C.; Aliaga, C.; Domínguez, M. The Inverted Solvatochromism of Protonated Ferrocenylethenyl-Pyrimidines: The First Example of the Solvatochromic Reversal of a Hybrid Organic/Inorganic Dye. *Org. Chem. Front.* **2019**, *6*, 3896–3901.

(3) Achelle, S.; Baudequin, C. Recent Advances in Pyrimidine Derivatives as Luminescent, Photovoltaic and Ono-Linear Optical Materials. In *Targets in Heterocyclic Systems*; Italian Chemical Society, 2013; Vol. 17, pp 1–34.

(4) Wang, W.-Y.; Ma, N.-N.; Wang, L.; Zhu, C.-L.; Fang, X.-Y.; Qiu, Y.-Q. Effect of π-Conjugate Units on the Ferrocene-Based Complexes: Switchable Second Order Nonlinear Optics Controlled by Redox Stimuli. *Dyes Pigm.* **2016**, *126*, 29–37.

(5) Fecková, M.; le Poul, P.; Bureš, F.; Robin-le Guen, F.; Achelle, S. Nonlinear Optical Properties of Pyrimidine Chromophores. *Dyes Pigm.* **2020**, *182*, 108659.

(6) Hildebrandt, A.; Schaarschmidt, D.; Lang, H. Electronically Intercommunicating Iron Centers in Di- and Tetraferrocenyl Pyrroles. *Organometallics* **2011**, *30*, 556–563.

(7) Maligaspe, E.; Pundsack, T. J.; Albert, L. M.; Zatsikha, Y. V.; Solntsev, P. V.; Blank, D. A.; Nemykin, V. N. Synthesis and Charge-Transfer Dynamics in a Ferrocene-Containing Organoboryl Aza-BODIPY Donor–Acceptor Triad with Boron as the Hub. *Inorg. Chem.* **2015**, *54*, 4167–4174.

(8) Zatsikha, Y. V.; Holstrom, C. D.; Chanawanno, K.; Osinski, A. J.; Ziegler, C. J.; Nemykin, V. N. Observation of the Strong Electronic Coupling in Near-Infrared-Absorbing Tetraferrocene Aza-Dipyrromethene and Aza-BODIPY with Direct Ferrocene−α- and Ferrocene−β-Pyrrole Bonds: Toward Molecular Machinery with Four-Bit Information Storage Capacity. *Inorg. Chem.* **2017**, *56*, 991–1000.

(9) Zatsikha, Y. V.; Shamova, L. I.; Schaffner, J. W.; Healy, A. T.; Blesener, T. S.; Cohen, G.; Wozniak, B.; Blank, D. A.; Nemykin, V. N. Probing Electronic Communication and Excited-State Dynamics in the Unprecedented Ferrocene-Containing Zinc MB-DIPY. *ACS Omega* **2020**, *5*, 28656–28662.

(10) Hildebrandt, A.; Schaarschmidt, D.; Claus, R.; Lang, H. Influence of Electron Delocalization in Heterocyclic Core Systems on the Electrochemical Communication in 2,5-Di- and 2,3,4,5-Tetraferrocenyl Thiophenes, Furans, and Pyrroles. *Inorg. Chem.* **2011**, *50*, 10623–10632.

(11) Hildebrandt, A.; Lang, H. (Multi)Ferrocenyl Five-Membered Heterocycles: Excellent Connecting Units for Electron Transfer Studies. *Organometallics* **2013**, *32*, 5640–5653.

(12) Connelly, N. G.; Geiger, W. E. Chemical Redox Agents for Organometallic Chemistry. *Chem. Rev.* **1996**, *96*, 877–910.

(13) Iyoda, M.; Kondo, T.; Okabe, T.; Matsuyama, H.; Sasaki, S.; Kuwatani, Y. A Simple and Efficient Synthesis of Di-, Tri-, and Tetraferrocenylarenes. *Chem. Lett.* **1997**, *26*, 35–36.

(14) Pfaff, U.; Hildebrandt, A.; Schaarschmidt, D.; Hahn, T.; Liebing, S.; Kortus, J.; Lang, H. Di- and Triferrocenyl (Hetero)Aromatics: Synthesis, Characterization, (Spectro-)Electrochemistry, and Calculations. *Organometallics* **2012**, *31*, 6761–6771.

(15) Yuan, K.; Wang, X.; Mellerup, S. K.; Wyman, I.; Schatte, G.; Ding, Z.; Wang, S. Triarylborane-Supported Polyferrocenyl Systems: Impact of the Linking Unit on Electronic and Electrochemical Properties. *Organometallics* **2016**, *35*, 3051–3059.
(16) Zatsikha, Y. V.; Blesener, T. S.; King, A. J.; Healy, A. T.; Goff, P. C.; Didukh, N. O.; Blank, D. A.; Kovtun, Y. P.; Nemykin, V. N. Fully Conjugated Pyrene–BODIPY and Pyrene–BODIPY–Ferrocene Dyads and Triads: Synthesis, Characterization, and Selective Noncovalent Interactions with Nanocarbon Materials. *J. Phys. Chem. B* **2021**, *125*, 360–371.
(17) Carter, C.; Kratish, Y.; Jurca, T.; Gao, Y.; Marks, T. J. Bis-Ferrocenyl-Pyridinediimine Trinuclear Mixed-Valent Complexes with Metal-Binding Dependent Electronic Coupling: Synthesis, Structures, and Redox-Spectroscopic Characterization. *J. Am. Chem. Soc.* **2020**, *142*, 18715–18729.
(18) Achelle, S.; Barsella, A.; Baudequin, C.; Caro, B.; Robin-le Guen, F. Synthesis and Photophysical Investigation of a Series of Push–Pull Arylvinyldiazine Chromophores. *J. Org. Chem.* **2012**, *77*, 4087–4096.
(19) Chupakhin, O. N.; Utepova, I. A.; Kovalev, I. S.; Rusinov, V. L.; Starikova, Z. A. Direct C-C Coupling of Ferrocenyllithium and Azaheterocycles by Nucleophilic Substitution of Hydrogen - Synthesis of Mono- and 1,1'-Diazinylferrocenes. *Eur. J. Org. Chem.* **2007**, 857–862.
(20) Xu, C.; Zhang, Y.-P.; Wang, Z.-Q.; Fu, W.-J.; Hao, X.-Q.; Xu, Y.; Ji, B.-M. Design and Synthesis of Tetranuclear Cluster Monophosphine-Cyclopalladated Ferrocenylpyrimidinone Complexes from the Palladium-Catalyzed Hydroxylation of Chloropyrimidine. *Chem. Commun.* **2010**, *46*, 6852–6854.
(21) Xu, C.; Li, H.; Wang, Z.; Lou, X.; Fu, W. Synthesis, Characterization, and Crystal Structures of Aryl-Substituted Ferrocenylpyrimidines by Site-Selective Stepwise Couplings of 2,4,6-Trichloropyrimidine. *Monatsh. Chem.* **2014**, *145*, 767–773.
(22) Li, S. H.; Zhao, Y. Hydrothermal Synthesis and Crystal Structure of (4-Piperidine-2-Pyrimidine)Ferrocene. *Asian J. Chem.* **2014**, *26*, 4923–4924.
(23) Abashev, G. G.; Antuf'eva, A. D.; Bushueva, A. Yu.; Kudryavtsev, P. G.; Osorgina, I. V.; Syutkin, R. V.; Shklyaeva, E. V. Ferrocenes Conjugated with Thiophene, Carbazole, and Pyrimidine Fragments: Synthesis and Properties. *Russ. J. Appl. Chem.* **2010**, *83*, 1435–1439.
(24) Zou, Y.; Zhang, Q.; Showkot Hossain, A. M.; Li, S.-L.; Wu, J.-Y.; Ke, W.-Z.; Jin, B.-K.; Yang, J.-X.; Zhang, S.-Y.; Tian, Y.-P. Synthesis, Crystal Structures, Electrochemistry and Nonlinear Optical Properties of a Novel (D–A–D) Biferrocenyl Derivative: 2-Amino-4,6-Diferrocenylpyrimidine. *J. Organomet. Chem.* **2012**, *720*, 66–72.
(25) Maji, M.; Panja, D.; Borthakur, I.; Kundu, S. Recent Advancement on Sustainable Synthesis of N-Heterocycles Following Acceptorless Dehydrogenative Coupling Protocol Using Alcohols. *Org. Chem. Front.* **2021**, *Advanced Article*.
(26) Hughes, G.; Wang, C.; Batsanov, A. S.; Fern, M.; Frank, S.; Bryce, M. R.; Perepichka, I. F.; Monkman, A. P.; Lyons, B. P. New Pyrimidine- and Fluorene-Containing Oligo(Arylene)s: Synthesis, Crystal Structures, Optoelectronic Properties and a Theoretical Study. *Org. Biomol. Chem.* **2003**, *1*, 3069–3077.
(27) Berner, D.; Klein, C.; Nazeeruddin, M. K.; De Angelis, F.; Castellani, M.; Bugnon, P.; Scopelliti, R.; Zuppiroli, L.; Graetzel, M. Efficient Blue Light-Emitting Diodes Based on a

Classical “Push-Pull” Architecture Molecule 4,4’-Di-(2-(2,5-Dimethoxyphenyl)Ethenyl)-2,2’-Bipyridine. *J. Mater. Chem.* **2006**, *16*, 4468–4474.
(28) Shaker, M.; Lee, J.-H.; Trinh, C. K.; Kim, W.; Lee, K.; Lee, J.-S. A Facile Method to Synthesize [A’(D’AD)2]-Based Push-Pull Small Molecules for Organic Photovoltaics. *RSC Adv.* **2015**, *5*, 66005–66012.
(29) Raheem, A. A.; Kamaraj, S.; Sannasi, V.; Praveen, C. New D-π-A Push-Pull Chromophores as Low Band Gap Molecular Semiconductors for Organic Small Molecule Solar Cell Applications. *Org. Chem. Front.* **2018**, *5*, 777–787.
(30) Song, C.; Wang, Z.; Li, J.; Chen, Y.; Zhao, F.; Zhang, H. Extension of π-Conjugation and Enhancement of Electron-Withdrawing Ability at Terminal Indenedione for A-π-D-π-A Small Molecules for Application in Organic Solar Cells. *Org. Electron.* **2020**, *81*, 105679.
(31) Kumar, C.; Raheem, A. A.; Pandian, K.; Nandakumar, V.; Shanmugam, R.; Praveen, C. Fine-Tuning the Optoelectronic Chattels of Fluoreno-Thiophene Centred Molecular Semiconductors through Symmetric and Asymmetric Push-Pull Switch. *New J. Chem.* **2019**, *43*, 7015–7027.
(32) Kato, S.-I.; Yamada, Y.; Hiyoshi, H.; Umezu, K.; Nakamura, Y. Series of Carbazole–Pyrimidine Conjugates: Syntheses and Electronic, Photophysical, and Electrochemical Properties. *J. Org. Chem.* **2015**, *80*, 9076–9090.
(33) Pérez-Caaveiro, C.; Oliva, M. M.; López Navarrete, J. T.; Pérez Sestelo, J.; Martínez, M. M.; Sarandeses, L. A. Synthesis of D–A–A and D–A–D Pyrimidine π-Systems Using Triorganoindium Reagents: Optical, Vibrational, and Electrochemical Studies. *J. Org. Chem.* **2019**, *84*, 8870–8885.
(34) Deibl, N.; Ament, K.; Kempe, R. A Sustainable Multicomponent Pyrimidine Synthesis. *J. Am. Chem. Soc.* **2015**, *137*, 12804–12807.
(35) Mastalir, M.; Glatz, M.; Pittenauer, E.; Allmaier, G.; Kirchner, K. Sustainable Synthesis of Quinolines and Pyrimidines Catalyzed by Manganese PNP Pincer Complexes. *J. Am. Chem. Soc.* **2016**, *138*, 15543–15546.
(36) Deibl, N.; Kempe, R. Manganese-Catalyzed Multicomponent Synthesis of Pyrimidines from Alcohols and Amidines. *Angew. Chem., Int. Ed.* **2017**, *56*, 1663–1666.
(37) Maji, M.; Kundu, S. Cooperative Ruthenium Complex Catalyzed Multicomponent Synthesis of Pyrimidines. *Dalton Trans.* **2019**, *48*, 17479–17487.
(38) Mondal, R.; Sinha, S.; Das, S.; Chakraborty, G.; Paul, N. D. Iron Catalyzed Synthesis of Pyrimidines Under Air. *Adv. Synth. Catal.* **2020**, *362*, 594–600.
(39) Chakraborty, G.; Sikari, R.; Mondal, R.; Mandal, S.; Paul, N. D. Nickel-Catalyzed Synthesis of Pyrimidines via Dehydrogenative Functionalization of Alcohols. *Asian J. Org. Chem.* **2020**, *9*, 431–436.
(40) Sultana Poly, S.; Siddiki, S. M. A. H.; Touchy, A. S.; Ting, K. W.; Toyao, T.; Maeno, Z.; Kanda, Y.; Shimizu, K. Acceptorless Dehydrogenative Synthesis of Pyrimidines from Alcohols and Amidines Catalyzed by Supported Platinum Nanoparticles. *ACS Catal.* **2018**, *8*, 11330–11341.
(41) Mondal, R.; Lozada, I. B.; Stotska, O.; Herbert, D. E. Catalytic Synthesis of Luminescent Pyrimidines via Acceptor-Less Dehydrogenative Coupling. *J. Org. Chem.* **2020**, *85*, 13747–13756.
(42) Mondal, R.; Herbert, D. E. Synthesis of Pyridines, Quinolines, and Pyrimidines via Acceptorless Dehydrogenative Coupling Catalyzed by a Simple Bidentate P^N Ligand Supported Ru Complex. *Organometallics* **2020**, *39*, 1310–1317.

(43) Armstrong, A. T.; Smith, F.; Elder, E.; McGlynn, S. P. Electronic Absorption Spectrum of Ferrocene. *J. Chem. Phys.* **1967**, *46*, 4321–4328.
(44) Gray, H. B.; Sohn, Y. S.; Hendrickson, N. Electronic Structure of Metallocenes. *J. Am. Chem. Soc.* **1971**, *93*, 3603–3612.
(45) Geiger, W. E.; Barriere, F. Organometallic Electrochemistry Based on Electrolytes Containing Weakly-Coordinating Fluoroarylborate Anions. *Acc. Chem. Res.* **2010**, *43*, 1030–1039.
(46) Zatsikha, Y. V.; Maligaspe, E.; Purchel, A. A.; Didukh, N. O.; Wang, Y.; Kovtun, Y. P.; Blank, D. A.; Nemykin, V. N. Tuning Electronic Structure, Redox, and Photophysical Properties in Asymmetric NIR-Absorbing Organometallic BODIPYs. *Inorg. Chem.* **2015**, *54*, 7915–7928.
(47) Winter, R. F. Half-Wave Potential Splittings ΔE1/2 as a Measure of Electronic Coupling in Mixed-Valent Systems: Triumphs and Defeats. *Organometallics* **2014**, *33*, 4517–4536.
(48) Herbert, D. E.; Gilroy, J. B.; Chan, W. Y.; Chabanne, L.; Staubitz, A.; Lough, A. J.; Manners, I. Redox-Active Metallomacrocycles and Cyclic Metallopolymers: Photocontrolled Ring-Opening Oligomerization and Polymerization of Silicon-Bridged [1]Ferrocenophanes Using Substitutionally-Labile Lewis Bases as Initiators. *J. Am. Chem. Soc.* **2009**, *131*, 14958–14968.
(49) Xu, G.-L.; Xi, B.; Updegraff, J. B.; Protasiewicz, J. D.; Ren, T. 1,6-Bis(Ferrocenyl)-1,3,5-Hexatriyne: Novel Preparation and Structural Study. *Organometallics* **2006**, *25*, 5213–5215.
(50) Fan, Y.; Li, H.-M.; Zou, G.-D.; Zhang, X.; Pan, Y.-L.; Cao, K.-K.; Zhang, M.-L.; Ma, P.-L.; Lu, H.-T. Diferrocenes Bridged by a Geminal Diethynylethene Scaffold with Varying Pendant Substituents: Electronic Interactions in Cross-Conjugated System. *Organometallics* **2017**, *36*, 4278–4286.
(51) Steckhan, E. Organic Syntheses with Electrochemically Regenerable Redox Systems. *Top. Curr. Chem.* **1987**, *142*, 1–69.
(52) Masson, G.; Herbert, D. E.; Whittell, G. R.; Holland, J. P.; Lough, A. J.; Green, J. C.; Manners, I. Synthesis and Reactivity of a Strained Silicon-Bridged [1]Ferrocenophanium Ion. *Angew. Chem., Int. Ed.* **2009**, *48*, 4961–4964.
(53) Cowan, D. O.; Kaufman, F. Organic Solid State. Electron Transfer in a Mixed Valence Salt of Biferrocene. *J. Am. Chem. Soc.* **1970**, *92*, 219–220.
(54) Cowan, D. O.; LeVanda, C.; Park, J.; Kaufman, Frank. Organic Solid State. VIII. Mixed-Valence Ferrocene Chemistry. *Acc. Chem. Res.* **1973**, *6*, 1–7.
(55) Robin, M. B.; Day, P. Mixed Valence Chemistry-A Survey and Classification. *Adv. Inorg. Chem. Radiochem.* **1968**, *10*, 247–422. https://doi.org/10.1016/S0065-2792(08)60179-X.
(56) Zatsikha, Y. V.; Nemez, D. B.; Davis, R. L.; Singh, S.; Herbert, D. E.; King, A. J.; Ziegler, C. J.; Nemykin, V. N. Testing the Limits of the BOPHY Platform: Preparation, Characterization, and Theoretical Modeling of BOPHYs and Organometallic BOPHYs with Electron-Withdrawing Groups at β-Pyrrolic and Bridging Positions. *Chem. - Eur. J.* **2017**, *23*, 14668.
(57) Salzner, U. Quantitatively Correct UV-Vis Spectrum of Ferrocene with TDB3LYP. *J. Chem. Theory Comput.* **2013**, *9*, 4064–4073.
(58) Brunel, F.; Lautard, C.; di Giorgio, C.; Garzino, F.; Raimundo, J.-M.; Bolla, J.-M.; Camplo, M. Antibacterial Activities of Mono-, Di- and Tri-Substituted Triphenylamine-Based Phosphonium Ionic Liquids. *Bioorg. Med. Chem. Lett.* **2018**, *28*, 926–929.

(59) Frisch, M. J.; Trucks, G. W.; Schlegel, H. B.; Scuseria, G. E.; Robb, M. A.; Cheeseman, J. R.; Scalmani, G.; Barone, V.; Petersson, G. A.; Nakatsuji, H.; Li, X.; Caricato, M.; Marenich, A. V.; Bloino, J.; Janesko, B. G.; Gomperts, R.; Mennucci, B.; Hratchian, H. P.; Ortiz, J. V.; Izmaylov, A. F.; Sonnenberg, J. L.; Williams-Young, D.; Ding, F.; Lipparini, F.; Egidi, F.; Goings, J.; Peng, B.; Petrone, A.; Henderson, T.; Ranasinghe, D.; Zakrzewski, V. G.; Gao, J.; Rega, N.; Zheng, G.; Liang, W.; Hada, M.; Ehara, M.; Toyota, K.; Fukuda, R.; Hasegawa, J.; Ishida, M.; Nakajima, T.; Honda, Y.; Kitao, O.; Nakai, H.; Vreven, T.; Throssell, K.; Montgomery, J. A.; Peralta, J. E.; Ogliaro, F.; Bearpark, M. J.; Heyd, J. J.; Brothers, E. N.; Kudin, K. N.; Staroverov, V. N.; Keith, T. A.; Kobayashi, R.; Normand, J.; Raghavachari, K.; Rendell, A. P.; Burant, J. C.; Iyengar, S. S.; Tomasi, J.; Cossi, M.; Millam, J. M.; Klene, M.; Adamo, C.; Cammi, R.; Ochterski, J. W.; Martin, R. L.; Morokuma, K.; Farkas, O.; Foresman, J. B.; Fox, D. J. *Gaussian 16, Revision B.01*; Gaussian 16, Revision B.01, Gaussian, Inc., Wallingford CT; Gaussian, Inc.: Wallingford CT, 2016.

(60) Becke, A. D. Density-Functional Thermochemistry. III. The Role of Exact Exchange. *J. Chem. Phys.* **1993**, *98*, 5648–5652.

(61) Lee, C.; Yang, W.; Parr, R.G. Development of the Colle-Salvetti Correlation-Energy Formula into a Functional of the Electron Density. *Phys. Rev. B Condens. Matter.* **1988**, *37*, 785–789.

(62) Becke, A. D. Density-Functional Exchange-Energy Approximation with Correct Asymptotic Behavior. *Phys. Rev. A* **1988**, *38*, 3098–3100.

(63) Perdew, J. P. Density-Functional Approximation for the Correlation Energy of the Inhomogeneous Electron Gas. *Phys. Rev. B* **1986**, *33*, 8822–8824.

(64) Wachters, A. J. H. Gaussian Basis Set for Molecular Wavefunctions Containing Third-Row Atoms. *J. Chem. Phys.* **1970**, *52*, 1033–1036.

(65) McLean, A. D.; Chandler, G. S. Contracted Gaussian Basis Sets for Molecular Calculations. I. Second Row Atoms, Z = 11-18. *J. Chem. Phys.* **1980**, *72*, 5639–5648.

(66) Zhao, Y.; Truhlar, D. G. The M06 Suite of Density Functionals for Main Group Thermochemistry, Thermochemical Kinetics, Noncovalent Interactions, Excited States, and Transition Elements: Two New Functionals and Systematic Testing of Four M06-Class Functionals and 12 Other Functionals. *Theor. Chem. Acc.* **2008**, *120*, 215–241.

(67) Tomasi, J.; Mennucci, B.; Cammi, R. Quantum Mechanical Continuum Solvation Models. *Chem. Rev.* **2005**, *105*, 2999–3094.

(68) Tenderholt, A. L. *QMForge: A Program to Analyze Quantum Chemistry Calculations*.

(69) Bruker-AXS. *APEX3 V2016.1-0*; Madison, Wisconsin, USA, 2016.

(70) Sheldrick, G. M. A Short History of SHELX. *Acta Cryst.* **2008**, *A64*, 112–122.

(71) Dolomanov, O. V.; Bourhis, L. J.; Gildea, R. J.; Howard, J. A. K.; Puschmann, H. OLEX2: A Complete Structure Solution, Refinement and Analysis Program. *J. Appl. Crystallogr.* **2009**, *42*, 339–341.

(72) Spek, A. L. *PLATON, A Multipurpose Crystallographic Tool*; Utrecht University: Utrecht, The Netherlands, 1998.